Selective hydrogenation of nitrobenzene to aniline in dense phase carbon dioxide over Ni/γ-Al$_2$O$_3$: Significance of molecular interactions

Xiangchun Meng [a,b], Haiyang Cheng [a], Yoshinari Akiyama [b], Yufen Hao [a], Weibin Qiao [a], Yancun Yu [a], Fengyu Zhao [a,*], Shin-ichiro Fujita [b], Masahiko Arai [b,*]

[a] State Key Laboratory of Electroanalytical Chemistry, Changchun Institute of Applied Chemistry, Chinese Academy of Sciences, Changchun 130022, China
[b] Division of Chemical Process Engineering, Graduate School of Engineering, Hokkaido University, Sapporo 060-8628, Japan

ARTICLE INFO

ABSTRACT

The selective hydrogenation of nitrobenzene (NB) over Ni/γ-Al$_2$O$_3$ catalysts was investigated using different media of dense phase CO$_2$, ethanol, and n-hexane. In dense phase CO$_2$, the total rate of NB hydrogenation was larger than that in organic solvents under similar reaction conditions; the selectivity to the desired product, aniline, was almost 100% over the whole conversion range of 0–100%. The phase behavior of the reactant mixture in/under dense phase CO$_2$ was examined at reaction conditions. *In situ* high-pressure Fourier transform infrared measurements were made to study the molecular interactions of CO$_2$ with the following reactant and reaction intermediates: NB, nitrosobenzene (NSB), and *N*-phenylhydroxylamine (PHA). Dense phase CO$_2$ strongly interacts with NB, NSB, and PHA, modifying the reactivity of each species and contributing to positive effects on the reaction rate and the selectivity to aniline. A possible reaction pathway for the hydrogenation of NB in/under dense phase CO$_2$ over Ni/γ-Al$_2$O$_3$ is also proposed.

© 2009 Elsevier Inc. All rights reserved.

1. Introduction

The catalytic hydrogenation of nitrobenzene (NB) is commonly used to manufacture aniline (AN), which is an important intermediate for polyurethanes, dyes, pharmaceuticals, explosives, and agricultural products [1]. In industrial processes, the reaction is generally carried out in the vapor phase over copper catalysts at above 240 °C [2,3]. It can also be performed in the liquid phase by using a variety of metal catalysts (Ni, Pt, and Pd) and organic solvents. Hydrogenation over Ni catalysts such as Raney Ni, Ni–B amorphous alloys, and Ni nanoparticles is generally carried out at 80–120 °C [3–5]. The noble metals (Pt and Pd) can catalyze the NB hydrogenation under milder conditions [3,6]; however, their use in large-scale production has not been practiced extensively due to their high costs. In addition, most previous reaction processes have one or more of the following problems: (1) the reaction mixture includes H$_2$ and organic compounds that could cause risk of explosion, (2) common organic solvents used are volatile and toxic, and (3) several poisonous reaction intermediates such as nitrosobenzene (NSB), *N*-phenylhydroxylamine (PHA), azoxybenzene (AOB), azobenzene (AB), and hydrazobenzene (HAB) are

formed along with the desired AN product (Scheme 1). The formation and accumulation of these undesired intermediates should be avoided for the green production of AN [10,11].

Supercritical carbon dioxide (scCO$_2$) is an attractive alternative to conventional organic solvents, due to its nonflammability, relative inertness, complete miscibility with gases, and easy separation from liquid/solid products after reactions [12–18]. Furthermore, scCO$_2$ can show interesting effects on reaction rates and product selectivity [19–25]. Recently the present authors studied the hydrogenation of NB in scCO$_2$ over noble metal catalysts including Pd, Pt, Ru, and Rh supported on carbon, silica, and alumina. Although the Pt/C catalyst was found to show the best performance [26,27], undesired intermediates were formed and accumulated during the reaction.

Thus, it remains to be a challenging task to achieve a high selectivity to AN for the hydrogenation of NB in green solvents over non-noble metal catalysts. In this work, the authors have studied the potential of conventional Ni/γ-Al$_2$O$_3$ catalysts for the hydrogenation of NB at 35 and 50 °C in the presence of dense phase CO$_2$ (herein, it means CO$_2$ gas pressurized to above or below its critical pressure). For comparison, the hydrogenation of NB was also examined in ethanol and *n*-hexane under similar reaction conditions. The presence of dense phase CO$_2$ not only enhanced the rate of NB hydrogenation but also improved the selectivity to the desired AN product. The roles of dense phase CO$_2$ are discussed

* Corresponding authors. Fax: +86 431 8526 2410 (F. Zhao), +81 11 706 6594 (M. Arai).
E-mail addresses: zhaofy@ciac.jl.cn (F. Zhao), marai@eng.hokudai.ac.jp (M. Arai).
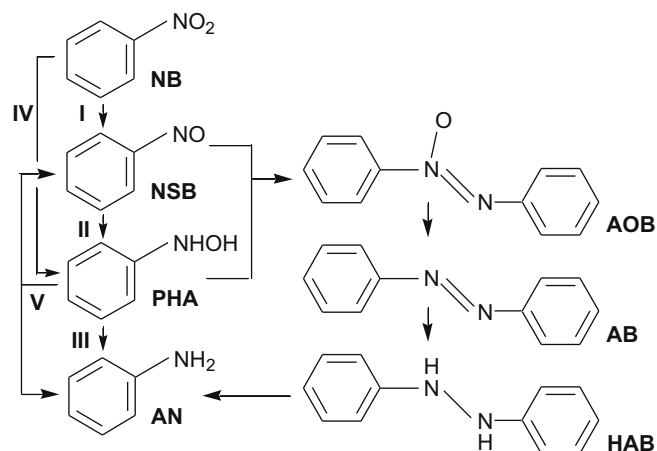
Scheme 1. Possible reaction pathways for the hydrogenation of nitrobenzene [7–9]. NB: nitrobenzene; NSB: nitrosobenzene; PHA: *N*-phenylhydroxylamine; AN: aniline; AOB: azoxybenzene; AB: azobenzene; HAB: hydrazobenzene.

on the basis of phase behavior observations and *in situ* high-pressure Fourier transform infrared (FTIR) measurements of the reacting species in CO_2. The molecular interactions of dense phase CO_2 with the reacting species (i.e., NB, NSB, and PHA) would be one of the important factors contributing to the enhanced reaction rate and product selectivity.

2. Experimental

2.1. Catalyst preparation and characterization

Two types of alumina-supported Ni catalysts were prepared by (a) incipient wetness impregnation using γ-alumina and $Ni(NO_3)_2 \cdot 6H_2O$ and (b) co-precipitation using $Ni(NO_3)_2 \cdot 6H_2O$ and $Al(NO_3)_3$ with a Ni/Al atomic ratio of 1/1. The two catalysts prepared via (a) and (b) are designated as IM-Ni/Al$_2$O$_3$ and CP-Ni/Al$_2$O$_3$, respectively.

The structural properties of catalysts were examined by X-ray diffraction (XRD, Philips PW1710 BASED) and transmission electron microscopy (TEM, JEM-2000EX). Temperature-programmed reduction (TPR) was carried out by heating a catalyst sample under 8% H$_2$/Ar at 8 K min^{-1} up to 850 °C.

A platinum/activated carbon catalyst (5 wt% Pt/C, Wako), in which the average size of Pt particles was ca. 3.7 nm (from XRD), was used for comparison.

2.2. Nitrobenzene hydrogenation

The hydrogenation of NB was examined over the two Ni/Al$_2$O$_3$ catalysts at 35 or 50 °C. The reaction runs in scCO$_2$ were conducted in a 50 cm^3 autoclave. The reactor was charged with NB 2.0 cm^3 (19.6 mmol) and a catalyst sample, flushed with N$_2$, and placed into a water bath preset to the reaction temperature for 20 min. After the introduction of H$_2$ (2.0–6.0 MPa), liquid CO$_2$ was introduced into the reactor with a high-pressure liquid pump (Jasco SCF-Get) to the desired pressure. The reaction was conducted while the reaction mixture was being stirred with a magnetic stirrer. After the reaction, the reactor was cooled with an ice-water bath for 20 min, depressurized carefully, and the reaction mixture was analyzed with a gas chromatograph (Shimadzu GC-14C, Rtx-wax capillary column) using a flame ionization detector. Hydrogenation reactions in ethanol and *n*-hexane were conducted in the same reactor using similar procedures.

2.3. Phase behavior and FTIR measurements

The phase behavior of the reactant mixture (i.e., NB and H$_2$) in the presence of dense phase CO$_2$ was examined by the naked eye through the transparent sapphire windows attached to an 85 cm^3 high-pressure reactor. The observations were made with a similar volumetric ratio of NB to the reactor volume as used in the hydrogenation runs. The details of experimental procedures were described elsewhere [20].

The high-pressure FTIR was used to examine the molecular interactions of CO$_2$ with reacting species. The FTIR spectra of NB, NSB, and PHA in dense phase CO$_2$ were collected with the same spectrometer in fashions similar to those collected in the previous work [28]. The measurements were made at 50 °C and in the presence of 0–20 MPa CO$_2$ and 4 MPa H$_2$. The weight of samples used was changed depending on its solubility in CO$_2$. A higher temperature of 78 °C was also used for PHA due to its low solubility. The liquid phase spectra were collected using the same spectrometer. For these measurements, NB and NSB (Sigma–Aldrich) were used as received; commercially unavailable PHA, one of the intermediates (Scheme 1), was synthesized according to the literature [29]. The formation of this compound was confirmed by FTIR and NMR (JEOL A200II) [30].

3. Results

3.1. Properties of Ni catalysts

The XRD patterns and TEM images of the two Ni catalysts are presented in Figs. 1 and 2, respectively; their features are summarized in Table 1. For the calcined IM-Ni/Al$_2$O$_3$ sample, the existence of NiO and γ-Al$_2$O$_3$ was identified. The TPR profile of IM-Ni/Al$_2$O$_3$ indicated two peaks centered at 420 and 520 °C (not shown), indicating that the formation of surface NiAl$_2$O$_4$ spinel was unlikely [31]. After reduction, Ni particles with diameters between 7 and 25 nm were formed, along with some aggregates in diameters >50 nm. The average Ni particle size was estimated to be 22 nm from the XRD line broadening. For CP-Ni/Al$_2$O$_3$, the co-precipitated precursor exhibited the XRD characteristic of nickel aluminum carbonate hydroxide, i.e., NiAl(CO$_3$)(OH)$_3$ (PDF No. 48-0593), but its
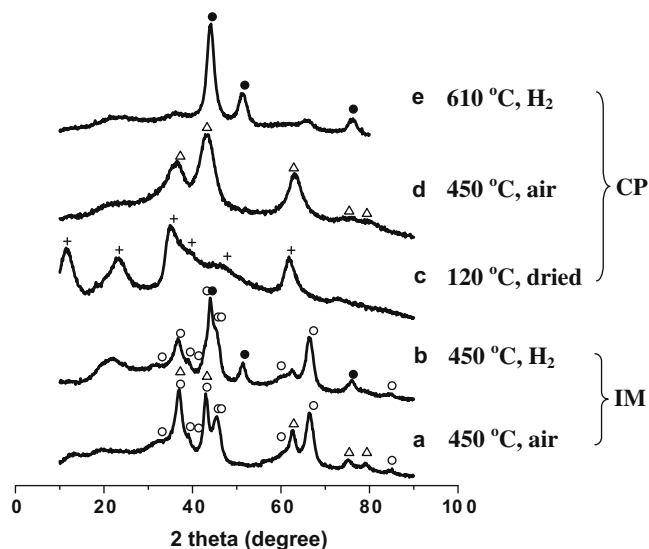

Fig. 1. XRD patterns of the IM- and CP-Ni/Al$_2$O$_3$ samples. IM sample: (a) calcined at 450 °C under air, (b) reduced at 450 °C with H$_2$; CP sample: (c) precursor dried at 120 °C, (d) calcined at 450 °C under air, (e) reduced at 610 °C with H$_2$. (○) γ-Al$_2$O$_3$; (△) NiO; (+) NiAl(CO$_3$)(OH)$_3$; (●) Ni.
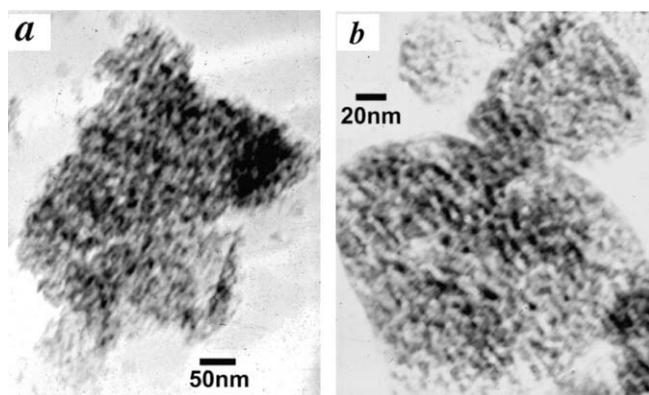
Fig. 2. TEM images of the reduced catalysts: (a) IM-Ni/Al$_2$O$_3$ (450 °C) and (b) CP-Ni/Al$_2$O$_3$ (610 °C).

crystallinity was somewhat poor. After calcination, the sample showed the broad NiO diffraction; no Al$_2$O$_3$ and NiAl$_2$O$_4$ spinel were identified, indicating that Al species were likely to be well mixed in the bulk of NiO [32]. After reduction, Ni particles in size mostly between 2 and 15 nm were formed. The average particle size determined from the XRD line broadening was ca. 8.5 nm, much smaller than that of the IM sample.

3.2. Hydrogenation performance

Table 2 shows the influence of reaction media on the hydrogenation of NB. After 50 min of reaction over IM-Ni/Al$_2$O$_3$, the conversion of NB in scCO$_2$ was much higher than that in ethanol and slightly higher than that of a solvent-free reaction system, although the NB concentration in scCO$_2$ was 1/5 of that in ethanol. Furthermore, the selectivity to AN (99%) was the highest in scCO$_2$ (entries 1–3). With CP-Ni/Al$_2$O$_3$, reactions in scCO$_2$ and in ethanol

Table 1
Alumina-supported Ni catalysts prepared and used for the hydrogenation of NB.

Sample	Ni loading[a] (wt%)	Phases present[b]		Ni crystallite size (nm)		TPR results[c] (°C)		
		Before reduction[d]	After reduction[d]	XRD	TEM[e]	T_{start}	T_{center}	T_{end}
IM-Ni/Al$_2$O$_3$	16	NiO, γ-Al$_2$O$_3$[f]	Ni, γ-Al$_2$O$_3$	22[g]	7–25, >50	332	420, 515	710
CP-Ni/Al$_2$O$_3$	41	NiO[h]	Ni[h]	8.5[g]	2–15	371	555	798

[a] In the calcined samples measured by inductively coupled plasma optical emission spectrometry.
[b] Detected by XRD.
[c] T_{start}, T_{center}, and T_{end} indicate the starting temperature of hydrogen consumption, the peak temperature, and the temperature at which no hydrogen consumption occurs during TPR, respectively.
[d] Reduced at 450 °C for IM-Ni/Al$_2$O$_3$ and 610 °C for CP-Ni/Al$_2$O$_3$.
[e] See Fig. 2.
[f] NiAl$_2$O$_4$ spinel was unlikely to form from TPR result.
[g] From (2 0 0) and (1 1 1) diffraction line broadening for IM-Ni/Al$_2$O$_3$ and CP-Ni/Al$_2$O$_3$, respectively.
[h] No clear diffraction due to Al$_2$O$_3$ and NiAl$_2$O$_4$ was detected.

Table 2
Hydrogenation of NB in scCO$_2$ and in organic solvents on Ni/Al$_2$O$_3$ and Pt/C catalysts.

Entry	Medium	P_{H2} (MPa)	Time (min)	Conv. (%)	Selectivity (%)		C_0[a] (mmol cm^{-3})	TOF[b] (h^{-1})
					AN	Byprod.[c]		
(a) *IM-Ni/Al$_2$O$_3$*								
1	Ethanol	4	50	13	89	11	1.96	81 (72)
2	Solv.-free	4	50	58	97	3	9.78	363 (352)
3	scCO$_2$	4	50	73	99	1	0.39	456 (451)
(b) *CP-Ni/Al$_2$O$_3$*								
4	Ethanol	2	30	30	81	19	1.96	141 (114)
5		4	30	36	78	22	1.96	170 (133)
6[d]		4	50	25	81	19	0.39	71 (58)
7		4	50	63	62	38	1.96	178 (110)
8		6	30	65	68	32	1.96	306 (208)
9	scCO$_2$	2	30	25	>99	<1	0.39	118 (117)
10		4	30	44	>99	<1	0.39	207 (206)
11[e]		4	50	42	>98	<2	9.78	119 (117)
12		4	50	68	>99	<1	0.39	193 (192)
13		6	30	56	>99	<1	0.39	264 (263)
14	Hexane	4	50	53	>98	<2	1.96	150 (148)
(c) *Pt/C*[f]								
15	scCO$_2$	6	25	72	75	25	0.39	87 870 (65 903)
16		6	45	98	78	22	0.39	–

Reaction conditions: 50 °C, NB 2.0 cm^3 (19.6 mmol), reactor 50 cm^3, IM-Ni/Al$_2$O$_3$ 0.3 g, or CP-Ni/Al$_2$O$_3$ 0.1 g, CO$_2$ 12 MPa or organic solvents 10.0 cm^3.
[a] Initial concentration of NB, mmol cm^{-3}.
[b] Turnover frequency of NB hydrogenation, which was given as the overall rate of NB conversion normalized by the number of active sites over the specified time; values in parentheses indicate TOF values of the hydrogenation of NB into AN. The number of active sites was calculated using the average Ni diameters (d) via the following equation: Dispersion = $6(v_m/a_m)/d$, where v_m and a_m are equal to 10.95 Å^3 and 6.51 Å^2, respectively, for Ni [33].
[c] Byproducts in ethanol mainly consist of NSB, AOB, PHA, and AB; a trace of AOB was detected in scCO$_2$.
[d] Ethanol 50 cm^3, reactor 100 cm^3.
[e] CO$_2$ 8 MPa, CO$_2$ expanded NB.
[f] Pt/C 0.005 g, 35 °C, NB 2.0 cm^3 (19.6 mmol), CO$_2$ 9 MPa.

were first carried out with an identical initial NB concentration (entries 6 and 12). Higher values of conversion (68%) and selectivity (>99%) were obtained in $scCO_2$ than (25% and 81%) in ethanol, similar to the results of $IM-Ni/Al_2O_3$. The selectivity to AN was >99% in $scCO_2$ at 2, 4, and 6 MPa H_2 and at any initial NB concentration used (entries 9–13); in contrast, the selectivity in ethanol changed between 62% and 81% with H_2 pressure (entries 4–8). Moreover, while the selectivity to AN was similar in $scCO_2$ and in apolar n-hexane (>98%), the conversion in the former (68%) was larger than that in the latter (53%) even though the NB initial concentration in $scCO_2$ was 1/5 of that in hexane (entries 12 and 14).

Table 2 also gives the turnover frequencies (TOFs) for the hydrogenation of NB into AN, showing that the TOFs were larger in $scCO_2$ than that in ethanol over both the Ni/Al_2O_3 catalysts (e.g., entries 1 and 3; 6 and 12). The TOF value in $scCO_2$ was also larger than that in hexane (entries 12 and 14). Thus, $scCO_2$ is a promising medium for the selective hydrogenation of NB to AN over Ni/Al_2O_3 catalysts, and the combination of $scCO_2$ and Ni/Al_2O_3 is better than that of $scCO_2$ and Pt/C (entries 15 and 16).

Table 2 shows that $IM-Ni/Al_2O_3$ was less active than $CP-Ni/Al_2O_3$ in ethanol (entries 1 and 7), but in $scCO_2$, the former was more active than the latter (entries 3 and 12). This indicates that dense phase CO_2 should have different extents of positive effects on the two Ni/Al_2O_3 samples.

Fig. 3 shows the evolution of product species with time during the hydrogenation of NB in ethanol and in $scCO_2$ over $CP-Ni/Al_2O_3$.
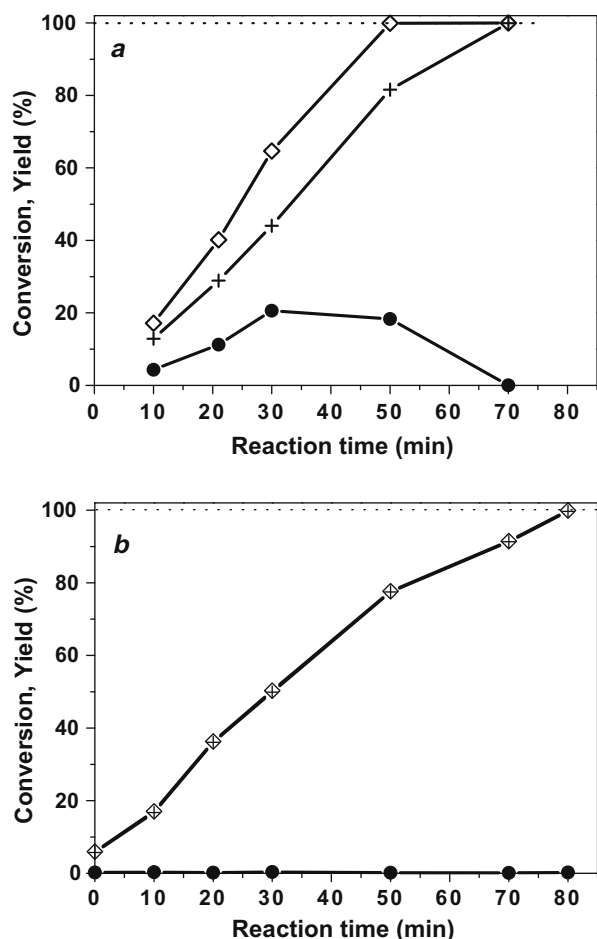

Fig. 3. Evolution of species with time during the hydrogenation of NB in ethanol (a) and in $scCO_2$ (b) over $CP-Ni/Al_2O_3$. (◇) NB conversion; (+) AN yield; and (●) yield of all byproducts. (Ethanol 10.0 cm^3 or CO_2 13.8 MPa, 50 °C, NB 19.6 mmol, H_2 6 MPa, catalyst 0.1 g.)
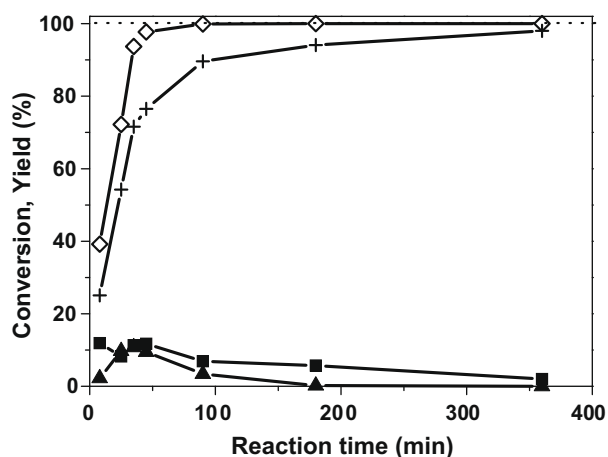

Fig. 4. Evolution of species with time during the hydrogenation of NB in $scCO_2$ over 5 wt% Pt/C. (◇) NB Conversion; (+) AN yield; (▲) NSB yield; and (■) yield of other byproducts including AOB, AB, and HAB. (CO_2 9 MPa, 35 °C, NB 19.6 mmol, H_2 6 MPa, Pt/C 0.005 g.)

AN was formed in a yield >99.5% in either ethanol or $scCO_2$ after 70 or 80 min, respectively. However, several intermediates were formed during the conversion of NB in ethanol (Fig. 3a). The intermediates included NSB, PHA, AOB, and AB (see Scheme 1). Although they could be further converted into AN given more time, their accumulation should be avoided because they are highly toxic and problematic [10,11]. It was reported that the addition of catalytic amounts of vanadium promoters could reduce the accumulation of PHA during the hydrogenation of aromatic nitro compounds over Pd or Pt catalysts [11]. For Ni catalysts used for the hydrogenation in organic solvents, however, the selection of effective promoters is difficult because modifiers that reduce the accumulation usually lower the reaction rate [34]. In this context, the present results of hydrogenation in $scCO_2$ over Ni/Al_2O_3 (Fig. 3b) are important because the reduction of intermediates could be accomplished along with an increase in reaction rates. The total yield of intermediates was <0.5% over the whole conversion range of 0–100%. To our best knowledge, such a selective hydrogenation of NB to AN over conventional Ni catalysts at mild temperatures has not been reported.

The present authors have shown that Pt/C is the better one among noble metal catalysts such as Pd, Pt, Ru, and Rh for the hydrogenation of NB in $scCO_2$ [26]. The results over Pt/C in $scCO_2$ are also included in Table 2 (entries 15 and 16). When compared on the basis of TOF, the Pt/C catalyst was much more active than the Ni/Al_2O_3 catalysts. However, the selectivity to AN on Pt/C was smaller (<80%) compared to that over Ni/Al_2O_3 (>99%). The undesired byproducts including NSB, AOB, AB, and HAB were formed during the hydrogenation of NB over Pt/C (Fig. 4). Although the conversion of NB was nearly completed in 45 min, these intermediates remained after 360 min. The poor selectivity to AN over Pt/C is not due to the lower reaction temperature (35 °C). The selectivity to AN is high over Ni/Al_2O_3 at both 50 and 35 °C, as shown later.

3.3. Influence of CO_2 pressure

Fig. 5a shows the influence of CO_2 pressure on the total conversion of NB over both $IM-Ni/Al_2O_3$ and $CP-Ni/Al_2O_3$ at 35 and 50 °C. The conversion increased first and then decreased with the introduction of CO_2. At 35 and 50 °C, the conversion was maximal at ca. 9 and 12 MPa CO_2, respectively. Fig. 5b shows the plot of the yield of AN against the conversion of NB at different CO_2 pressures. The selective hydrogenation of NB to AN could be achieved over
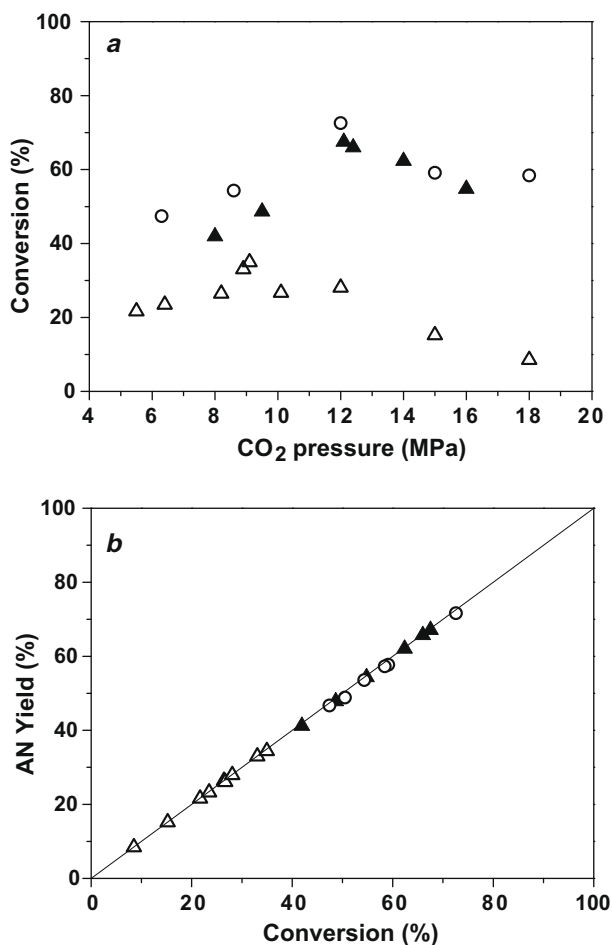
Fig. 5. Influence of CO_2 pressure on the conversion of NB (a) and correlation of AN yield against total NB conversion at different CO_2 pressures (b) during the NB hydrogenation in scCO₂ over IM-Ni/Al₂O₃ and CP-Ni/Al₂O₃ catalysts. (○) IM-Ni/Al₂O₃ 0.3 g, 50 °C; (▲) CP–Ni/Al₂O₃ 0.1 g, 50 °C; and (△) CP-Ni/Al₂O₃ 0.075 g, 35 °C. (H₂ 4 MPa, 50 min.)

the whole conversion range examined irrespective of CO_2 pressures and temperatures.

3.4. Phase behavior

Fig. 6 shows the photographs of visual observations on the state of the reactant mixture at different CO_2 pressures and temperatures. At 35 °C, the liquid NB gradually expanded with the introduction of CO_2 and transformed into a single gas phase at 10.5 MPa, above which NB was completely dissolved in CO_2. On
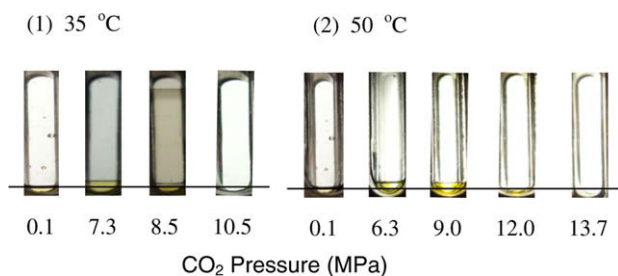

Fig. 6. Phase behavior of NB at 35 and 50 °C pressurized by 4 MPa H₂ and dense phase CO_2 at different pressures given. The relative volume of NB against the reactor volume was the same as used in the hydrogenation runs. The line across the pictures indicates the initial liquid–gas interface at 4 MPa H₂ and 0.1 MPa CO_2.

the careful depressurization, the cloud point was observed at 9.2 MPa CO_2. At 50 °C, the single phase and the cloud point appeared at 13.7 and 12.6 MPa CO_2, respectively. At both temperatures, the pressure for the maximum conversion (Fig. 5) is similar to that of the cloud point observed, indicating that the phase behavior is an important factor in determining the rate of NB hydrogenation. However, the high selectivity to AN remained unchanged when the reaction mixture changed from the gas–liquid–solid system to the gas–solid one.

3.5. FTIR measurements

(a) *NB*. Fig. 7 shows the FTIR spectra of nitro group vibrations in the presence of 4 MPa H₂ and 0–20 MPa CO_2. The FTIR results of NB in pure liquid phase and in ethanol (with the same ratio of NB to ethanol as used in the hydrogenation runs) are shown for comparison. The bands at ca. 1350 and 1524 cm^{-1} were assigned to the symmetric and asymmetric
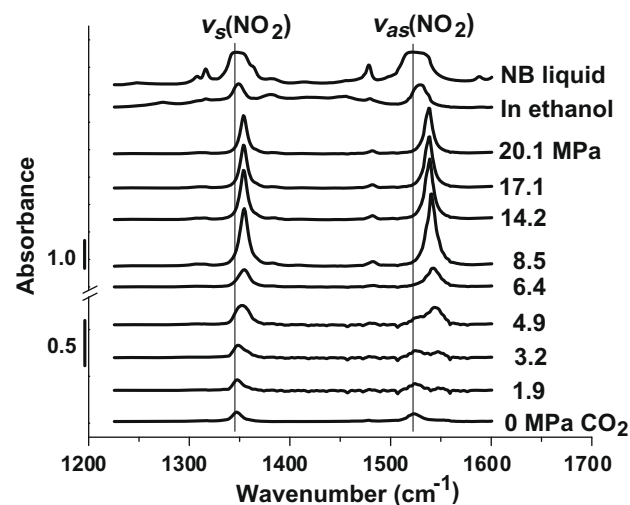

Fig. 7. FTIR spectra of nitro group stretching vibrations for NB in the presence of 4 MPa H₂ and dense phase CO_2 at different given pressures at 50 °C. Also included are the same group vibrations of NB in the liquid phase and in a mixture of NB and ethanol (NB/ethanol = 0.2, v/v) at room temperature.
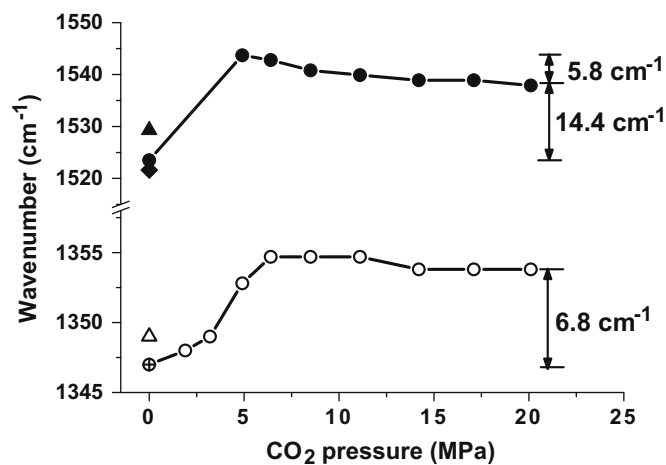

Fig. 8. FTIR results of the nitro group vibrations for NB. (○) Symmetric and (●) asymmetric stretching vibrations in dense phase CO_2 at 50 °C; (+) symmetric and (◆) asymmetric stretch in liquid phase; (△) symmetric and (▲) asymmetric stretch in a mixture of NB and ethanol (NB/ethanol = 0.2, v/v) at room temperature.
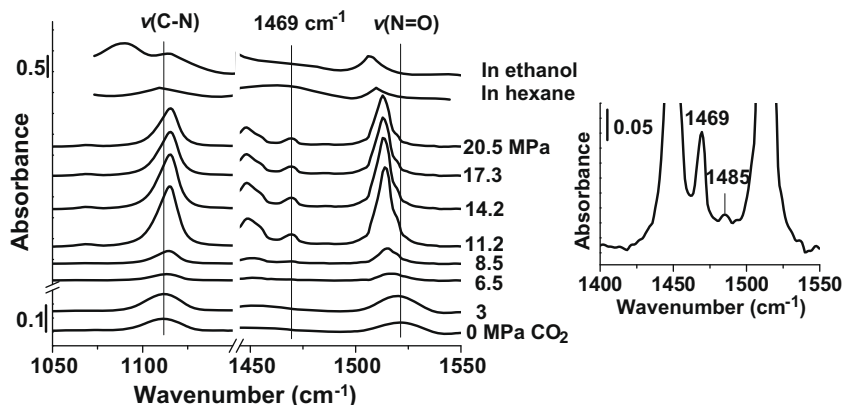
Fig. 9. FTIR spectra of NSB in the presence of 4 MPa H_2 and dense phase CO_2 at given pressures and at 50 °C. Also shown are the spectra of NSB in hexane (NSB saturated hexane) and in ethanol (NSB/ethanol = 0.11, molar ratio) at room temperature. The inset shows a magnified spectrum of NSB in dense phase CO_2 (20.5 MPa) to show the peak at 1485 cm^{-1}.

stretching vibrations of the nitro group, $v_s(NO_2)$ and $v_{as}(NO_2)$ [9]. The peaks of $v_s(NO_2)$ and $v_{as}(NO_2)$ appeared at different wavenumbers depending on CO_2 pressure, and these peak shifts are depicted in Fig. 8. At CO_2 pressures <5 MPa, two separate bands were detected for $v_{as}(NO_2)$ at 1524 and 1547 cm^{-1}, so no data are shown in Fig. 8. The peak positions of both $v_s(NO_2)$ and $v_{as}(NO_2)$ were blue shifted with CO_2 pressure up to ca. 6 MPa as compared to those in the ambient gas phase. At 6–20 MPa CO_2, these peak positions were slightly shifted to a lower wavenumber and then barely changed. The absorption bands at 20 MPa CO_2 were located at larger wavenumbers than those in the ambient gas state and in the liquid state (neat and in ethanol). These FTIR results indicate that the N–O bond of the nitro group becomes stronger in the presence of dense phase CO_2 compared to the ambient gas and liquid conditions. Additionally, an absorption band appeared at 1108 cm^{-1} in the gas phase before the introduction of CO_2 and was blue shifted to 1112 cm^{-1} with CO_2 pressure up to 6.4 MPa, above which it did not change further. This band is due to the C–N stretch [35].

(b) *NSB.* The FTIR spectra of the nitroso moiety of NSB were measured in dense phase CO_2 at different pressures and in the presence of 4 MPa H_2 at 50 °C (Fig. 9). The spectra of NSB dissolved in hexane and ethanol at room temperature were recorded for comparison. An absorption band due to the stretching vibration of $v(N=O)$ appeared at 1521 cm^{-1} before the introduction of CO_2, in accordance with the corresponding value of 1523 cm^{-1} in gas phase as reported previously [35,36]. It was reported that the absorption bands at 1412 and 1389 cm^{-1} are due to the symmetric and antisymmetric N=O stretch of *cis*-dimeric NSB and those at 1112 and 1190 cm^{-1} arise from the C–N stretch of the NSB monomer and dimer, respectively [36]. The absence of bands due to dimer in our IR spectra shows that NSB is present in the form of monomer in dense phase CO_2 at all pressures examined. The peak position of $v(C-N)$ of NSB monomer was slightly blue shifted from 1112 to 1116 cm^{-1} with the increase in CO_2 pressure up to 14 MPa. In addition, there was a very weak band located at 1485 ± 1 cm^{-1} at CO_2 pressures >8 MPa (the inset of Fig. 9). It has been reported that the N=O stretching bands of NSB occur around 1500 and 1484 cm^{-1} when NSB is coordinated in organometallic complexes or adsorbed on metal oxides. The band around 1500 cm^{-1} is related to the nitroso ligand coordinated through the oxygen atom to a low-valent metal center, while that at 1484 cm^{-1} is contributed by another coordination

mode of NSB through the nitrogen atom [36,37]. Thus, the bands around 1520 and 1485 cm^{-1} in our IR spectra would arise from the stretching vibration of N=O group that interacts with CO_2 molecules, respectively, through its oxygen (O-interacted) and nitrogen (N-interacted) atoms. Because the latter was very weak and its peak position did not change, we direct our attention to the former absorption band. The influence of pressure on the peak position of $v(N=O)$(O-interacted) absorption band is shown in Fig. 10. The wavenumber of the peaks followed the order of ambient gas state > in hexane > in ethanol. The stretching vibration of $v(N=O)$(O-interacted) in CO_2 was monotonously red shifted with CO_2 pressure up to 14 MPa and then remained unchanged. At 20 MPa CO_2, the peak position of $v(N=O)$(O-interacted) was at 1513 cm^{-1}, which was still higher than that in hexane or ethanol (1511 and 1507 cm^{-1}, respectively).

(c) *PHA.* The FTIR spectra of PHA in dense phase CO_2 and in ethanol are given in Fig. 11. The absorption bands at 925, 1494–1500, and 3120 cm^{-1} are related to the N–O stretch, a ring-stretching mode, and the O–H stretching vibration of PHA derivatives, respectively [38–40]. The O–H stretching band of PHA in dense phase CO_2 was not distinct at all pressures examined. The N–O stretch of PHA could not be identified at CO_2 pressures <8 MPa; at 8.5 MPa, its absorp-
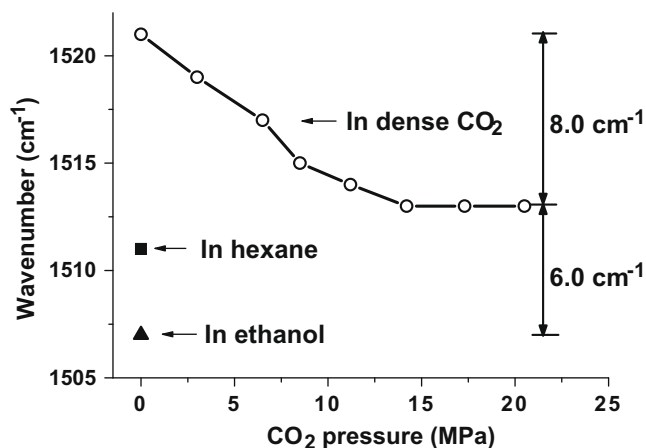

Fig. 10. Influence of CO_2 pressure on the peak position of the nitroso group (O-interacted) vibrations for NSB at 50 °C. Also shown are the same group vibrations in hexane (NSB saturated hexane) and in ethanol (NSB/ethanol = 0.11, molar ratio) at room temperature.
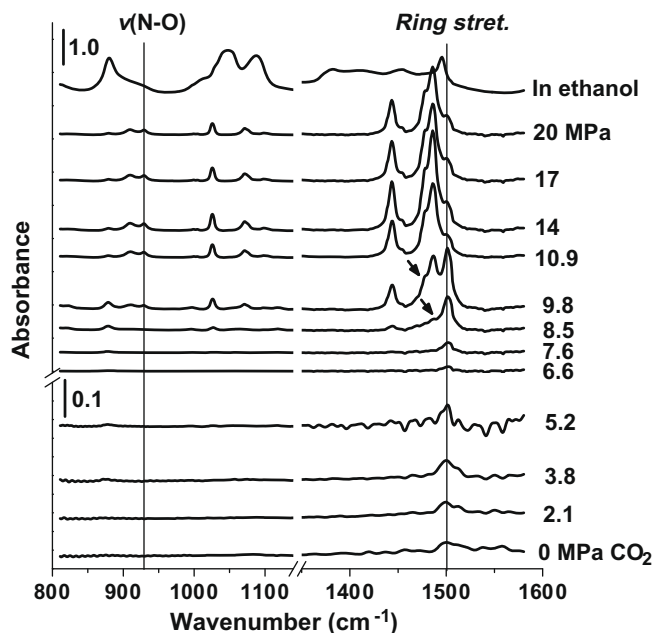
Fig. 11. FTIR spectra for the ring-stretching vibration of PHA in the presence of 4 MPa H_2 and dense phase CO_2 at given pressures. The spectra at pressures <4 MPa were collected at 78 °C and those at pressures >5 MPa at 50 °C. The spectrum of PHA in ethanol (PHA/ethanol = 0.26, molar ratio) collected at room temperature is also shown.

Fig. 12. Influence of CO_2 pressure (○) on the main peak position of the absorption band due to ring-stretching vibration for PHA (see Fig. 11 for measurement conditions). Also shown are the results for PHA in KBr (●) and in ethanol (PHA/ethanol = 0.26) (▲) measured at room temperature. The inset shows the deconvolution result of combination bands obtained at 14 MPa CO_2.

tion band was observed at 929 cm^{-1}. However, the peak position did not show any shift at CO_2 pressures from 8.5 to 20 MPa. Here, our interest is focused on the absorption band at 1500 ± 2 cm^{-1}, which is related to the ring stretch of PHA, for the discussion on interactions between PHA and CO_2 molecules.

The ring absorption band was weak and its peak position was difficult to be determined at CO_2 pressures <4 MPa (PHA 6 mg, 50 °C). The measurements using a larger amount of PHA (15 mg) and a higher temperature (78 °C) indicated that the peak position scarcely changed in the CO_2 pressure range of 0–4 MPa (Fig. 11). At 8.5 MPa CO_2, a shoulder could be seen, as indicated by arrow in Fig. 11; at 9.8 MPa, the absorption band split into three peaks: two distinct peaks along with a shoulder (as shown by arrow). Upon further increase in the CO_2 pressure, the absorption occurred in a range of smaller wavenumbers and split into a few absorption bands. The spectra collected at pressures >9 MPa were analyzed by deconvolution. There were three absorption bands centered at 1478, 1486, and 1501 cm^{-1} (see inset in Fig. 12). The influence of CO_2 pressure on the main peak position of the ring-stretching vibration is shown in Fig. 12. It scarcely changed with CO_2 pressure up to ca. 4 MPa, above which it was red shifted but remained unchanged from 11 to 20 MPa CO_2.

Interactions of CO_2 with Lewis base, polymer, or ionic liquids cause some changes in the IR spectra corresponding to the CO_2 v_2-bending mode region (610–680 cm^{-1}) and v_3-antisymmetric stretching (2100–2500 cm^{-1}) mode region [41–43]. It was impossible to distinguish the v_2 mode in our IR results. Fig. 13 shows the IR spectra of CO_2 in the v_3 region for the CO_2–PHA system at different pressures. The results shown in Fig. 13 were obtained by using the PHA-absent system at the corresponding pressures as background. At 3.5 MPa CO_2, the difference spectrum indicates that the v_3
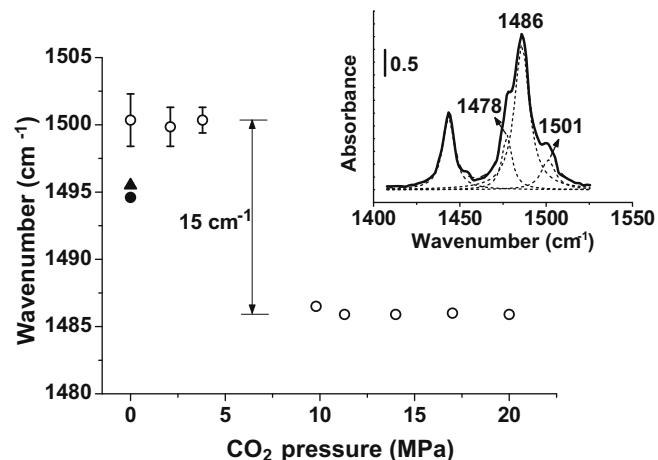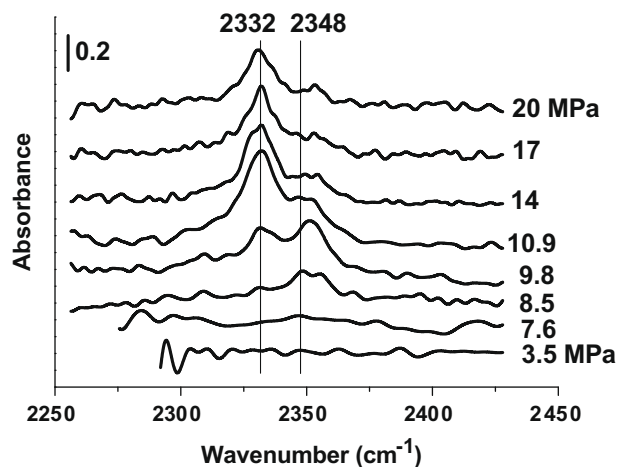

Fig. 13. FTIR difference spectra in the CO_2 v_3-antisymmetric stretching mode region for the CO_2–PHA system at given CO_2 pressures. All spectra were collected at 50 °C in the presence of 4 MPa H_2, and the difference spectra were obtained by using the PHA-absent system at the corresponding pressures as background.

mode stretch in the presence of PHA was similar to that in the absence of PHA. With CO_2 pressure increased up to 8.5 MPa, peaks appeared in the region of 2348–2355 cm^{-1}; at 9.8 MPa, an additional peak was clearly observed at 2332 cm^{-1}. The band at 2332 cm^{-1} showed little shift in peak position with CO_2 pressures up to 20 MPa. It is important to observe more than one band in the v_3 region. Spectral changes in the v_3 mode region give additional evidence for the interactions between PHA and CO_2 molecules under pressurized conditions.

4. Discussion

4.1. Improvement of the selectivity to AN

The FTIR results show that the strength of the N–O bond of NB in dense phase CO_2 was stronger than that in the ambient gas phase and it increased with CO_2 pressure up to ca. 6 MPa, above

which it slightly decreased (Fig. 8). However, the strength of the N=O bond of NSB was monotonously reduced with CO_2 pressure (Fig. 10). Namely, the reactivity of the $-NO_2$ group may decrease with CO_2 pressure up to 6 MPa and will not change so much at higher pressures. In contrast, the reactivity of the –NO group may increase with CO_2 pressure. It is likely, therefore, that the relative reactivity of the –NO group is higher than that of the $-NO_2$ one at any CO_2 pressure, indicating that the hydrogenation of NSB is more significantly accelerated than that of NB when dense phase CO_2 is used. Moreover, the FTIR results indicate that interactions occurred between PHA and dense phase CO_2 molecules. Different modes of interactions are possible, as will be discussed later, and these interactions should promote the transformation of PHA to AN (step III in Scheme 1), contributing to the improved selectivity to AN. As a result, AN was formed with almost 100% selectivity in/under dense phase CO_2. Therefore, the molecular interactions of CO_2 with the reacting species should be an important factor in determining the product selectivity. These interactions should also occur in the CO_2-expanded substrate phase because the concentration of CO_2 in this liquid phase is large under pressurized conditions.

The difference in the selectivity between Ni/Al$_2$O$_3$ and Pt/C catalysts in scCO$_2$ might be due to a large difference in their hydrogenation activities. The above-mentioned molecular interactions of reacting species with CO_2 are also effective for the reaction on Pt/C in scCO$_2$. In fact, it was reported that the selectivity to AN is improved in scCO$_2$ for the reaction over Pt/C [26]. Because the activity of Pt/C was much higher than that of Ni/Al$_2$O$_3$ (Table 2), the contribution of the molecular interactions to the rates of hydrogenation steps should be relatively less significant for Pt/C than for Ni/Al$_2$O$_3$ catalyst.

4.2. Modes of molecular interactions of CO_2

The carbon atom of CO_2 is partially positive and the oxygen atoms are partially negative [20]; CO_2 can act as both a Lewis acid (LA) through the carbon atom and a Lewis base (LB) through the oxygen atoms [44]. The CO_2 molecule could form, with aromatic compounds (π-electron donors), an electron donor–acceptor complex with parallel arrangement of the molecules [43,45].

(a) *NB.* The nitro group can strongly withdraw electrons from the aromatic ring by inductive and resonance effects, and the ring of NB is greatly deactivated toward an electrophilic attack [46,47]. Therefore, CO_2 interactions with π-electrons of the aromatic ring, if present, become less significant in the case of NB. The two oxygen atoms of NB are negatively charged, while the nitrogen is positively charged [47]. Our IR results illustrate that the absorption bands of the C–N and N–O stretching vibrations were blue shifted first with the introduction of CO_2 up to ca. 5–6 MPa, above which the former remained unchanged but the latter showed a slight red-shift. This means that the overall IR result of NB is controlled by two interaction modes between CO_2 molecules and the nitro group. Presumably, (1) one of the oxygen atoms of CO_2 interacts with the positive nitrogen of $-NO_2$ group and (2) the carbon atom of CO_2 interacts with the oxygen of $-NO_2$ group. The CO_2 molecule plays an LB role in the former and an LA role in the latter. It is expected that the former interaction might strengthen both the C–N and N–O bonds, while the latter might weaken the strength of the N–O bond. The IR results show that the former interaction has a dominant effect on the stretching vibration of N–O bond. Similar LA–LB interaction to the latter mode has been reported to occur between CO_2 and electron-donating organic compounds containing carbonyl

or sulfonyl group [42,48,49]. The bond strength of the carbonyl group is weakened by this type of molecular interaction, as evidenced by FTIR spectra and computational studies [20,28,49]. On the other hand, the high solubility of poly(dimethylsiloxane) in scCO$_2$ has been ascribed to the interactions of the oxygen electrons of CO_2 with Si atoms in the polymer chains [50].

(b) *NSB.* The nitroso group also definitely deactivates the ring toward an electrophilic attack; in contrast to the $-NO_2$ group, a feature of the –NO group is the retention of the nitrogen lone pair. The nitrogen and oxygen atoms have a higher electron density, which are both possible reactive sites toward electrophiles [51]. NSB can be coordinated/adsorbed to metal cations by N- as well as O-bonding [36,37]. Our IR results of NSB in dense phase CO_2 demonstrate that the absorption band of the O-interacted NSB was clearly detected at all pressures examined, and the N-interacted form could be only identified at above 8 MPa CO_2 with a very weak absorption. Thus, it is concluded that NSB dominantly interacts by its oxygen atom to the positively polarized carbon of CO_2. This type of intermolecular interaction becomes stronger with the increase in CO_2 pressure and it weakens the N=O bond of NSB. Simultaneously, the C–N stretching band was blue shifted, in agreement with the previous results for nitroso compounds that v(C–N) increases when v(N=O) decreases [36]. In the NSB/CO_2 interaction system, CO_2 plays a role of an LA and the –NO group functions as an LB. The wavenumber of v(N=O)(O-interacted) at 20 MPa CO_2 was still higher than that in ethanol (1507 cm^{-1}). The absorption band at 1507 cm^{-1} in ethanol is related to the stretch of N=O that interacts through the oxygen atom with the hydroxyl group of ethanol via hydrogen bonding [36]. Accordingly, the LA–LB interaction of CO_2 with the O-interacted –NO group is less strong compared with the hydrogen bonding in ethanol.

(c) *PHA.* There exist nitrogen and oxygen lone pairs on the hydroxylamino (–NH–OH) group of PHA. The –NH–OH group is a ring-activating electron donor; namely, the ring of PHA is activated toward an electrophilic attack [52]. Our IR spectra indicate that interactions occurred between the ring of PHA with dense phase CO_2 molecules and a stretching mode of the ring was split and red shifted. The CO_2 may interact with the π-electron system of phenyl ring through electrostatic interaction or by forming an electron donor–acceptor complex [42,43,45]. Computational study indicated that the oxygen, nitrogen, and ring of PHA might function as hydrogen bond acceptors, with the order of the accepting ability being O > N > ring; the hydroxyl H, amine H, and ring H of PHA may have hydrogen bond donating abilities, in the order hydroxyl H > amine H > ring H. The –NH–OH group of PHA is as effective hydrogen bond donors as H$_2$O. The basicity of the nitrogen lone pairs is similar to that of pyridine [52]. Meanwhile, CO_2 can act as either an LA or an LB. It can also interact with the –OH group by forming either an electron donor–acceptor complex or a hydrogen bond [53,54]. Thus, there are several possible modes for the interaction of PHA with CO_2 molecules: (i) LA–LB interaction between the positive carbon atom of CO_2 with the nitrogen, oxygen, or the ring of PHA and (ii) hydrogen bond formation between the oxygen atoms of CO_2 and the hydroxyl H, amine H, or ring H of PHA. The IR spectra of dense phase CO_2 in the v_3-mode region showed the occurrence of a few absorption bands in the presence of PHA. This indicates that two or more inequivalent sites within the PHA molecule could interact with CO_2 [42].

4.3. Reaction pathway for the hydrogenation of NB in dense phase CO_2 over Ni/γ-Al$_2$O$_3$

The path IV in Scheme 1 occurs on Au/TiO$_2$, and the step V becomes significant over Pd/Pt/Ni catalysts in the presence of vanadium promoters [9,11,34]. Herein, we discuss the different reaction pathways in dense phase CO_2 and in ethanol without the consideration of pathways IV and V.

With Ni/γ-Al$_2$O$_3$ catalysts in ethanol, many byproducts including NSB, PHA, AOB, and AB were formed and the rate of AN formation was much lower than the rate of NB transformation (entries 4–8, Table 2). Hence, AN is formed via both the direct hydrogenation route (steps I → II → III) and the condensation one (right pathway in Scheme 1), and the hydrogenation of NB to NSB (step I) is relatively fast.

With the same catalyst in dense phase CO_2, the yield of byproducts was <0.5% over the whole conversion range of 0–100% (Fig. 3b). Accordingly, the condensation route in Scheme 1 should be negligible, and the hydrogenation of NB to AN proceeds likely through the consecutive steps I → II → III. The rate of AN formation should be determined by the slowest reaction rate among steps I–III. As shown above, the rate of AN formation was almost equal to that of NB conversion, i.e., the rate of step I (entries 9–13, Table 2); the yield of AN showed a strong dependence on the phase behavior of NB (see Section 3.3 and 3.4); the high selectivity to AN remained unchanged with increasing CO_2 pressure (Fig. 5). Therefore, in the case of NB hydrogenation in dense phase CO_2 over Ni/γ-Al$_2$O$_3$, the transformation of NB to NSB (step I in Scheme 1) seems to be the relatively slow step that determines the rate of AN formation.

The proposed reaction pathway may be related to the molecular interactions of CO_2 with NB, NSB, and PHA. The relative reactivity of these reacting species was changed as discussed above, and consequently, the relative hydrogenation rates of steps I–III are altered in dense phase CO_2.

The proposed pathway may explain why the rate of AN formation depends strongly on the NB phase behavior. At low pressures, the reaction occurs in the gas–liquid–solid three-phase system. When pressurized by CO_2, the NB liquid expands and the dissolution of H$_2$ is promoted. The conversion of NSB and PHA is accelerated because of the molecular interactions with CO_2. Hence, the rate of NB hydrogenation increases with CO_2 pressure. When the reaction takes place in a gas–solid system at higher pressures, the reactivity of the reacting species does not change so much when varying CO_2 pressure, but NB is dissolved and diluted in the gas phase. The diffusion coefficient of NB also decreases with the density of CO_2 [55]. These effects cause the decrease in the rate of NB hydrogenation with further pressurization with CO_2.

The above discussion does not exclude the possible interaction of CO_2 with the catalyst surface. For example, CO was detected in some scCO$_2$ reaction systems containing Pt-group metal catalysts [22,56,57]. The chemisorption of CO_2 on Ni surface could result in non-negligible electronic charge transfers from the metal to CO_2 [58]. Nevertheless, our results show that interactions of CO_2 with NB, NSB, and PHA are one of the important roles of CO_2 for the enhanced reaction rate and selectivity.

5. Conclusions

The multiphase reaction system using conventional Ni/Al$_2$O$_3$ catalysts and dense phase CO_2 enables the selective hydrogenation of nitrobenzene to aniline under mild conditions. The selectivity to the desired product, aniline, was almost 100% at any conversion level ranging from 0% to 100%. One of the important factors for this improved selectivity to aniline is the interactions of dense phase CO_2 with the reacting species (i.e., nitrobenzene, nitrosobenzene, and N-phenylhydroxylamine). The reactivity of nitrobenzene is decreased but that of nitrosobenzene is increased and the transformation of N-phenylhydroxylamine to aniline is likely promoted. Probably, the hydrogenation of nitrobenzene mainly occurs through the direct hydrogenation route, i.e., nitrobenzene → nitrosobenzene → N-phenylhydroxylamine → aniline. The transformation of nitrobenzene to nitrosobenzene might be the rate-determining step. The strong molecular interactions between the reactants and intermediates with the solvent may be also important during the selective hydrogenation of other nitro compounds to amines in dense phase CO_2.

References

[1] A.S. Travis, in: Z. Rappoport (Ed.), The Chemistry of Anilines, John Wiley and Sons, 2007, p. 715.
[2] S. Diao, W. Qian, G. Luo, F. Wei, Y. Wang, Appl. Catal. A 286 (2005) 30.
[3] S. Nishimura, Handbook of Heterogeneous Catalytic Hydrogenation for Organic Synthesis, John Wiley and Sons, 2001. p. 332.
[4] H. Li, Q. Zhao, Y. Wan, W. Dai, M. Qiao, J. Catal. 244 (2006) 251.
[5] R. Xu, T. Xie, Y. Zhao, Y. Li, Nanotechnology 18 (2007) 055602.
[6] V. Holler, D. Wegricht, I. Yuranov, L. Kiwi-Minsker, A. Renken, Chem. Eng. Technol. 23 (2000) 251.
[7] E.A. Gelder, S.D. Jackson, C.M. Lok, Chem. Commun. (2005) 522.
[8] H.U. Blaser, Science 313 (2006) 312.
[9] A. Corma, P. Concepcion, P. Serna, Angew. Chem., Int. Ed. 46 (2007) 7266.
[10] F. Cardenas-Lizana, S. Gomez-Quero, M.A. Keane, Appl. Catal. A 334 (2008) 199.
[11] P. Baumeister, H.U. Blaser, M. Studer, Catal. Lett. 49 (1997) 219.
[12] C.A. Eckert, B.L. Knutson, P.G. Debenedetti, Nature 383 (1996) 313.
[13] P.G. Jessop, W. Leitner, in: P.G. Jessop, W. Leitner (Eds.), Chemical Synthesis Using Supercritical Fluids, Wiley–VCH, Weinheim, Germany, 1999, p. 9.
[14] A. Baiker, Chem. Rev. 99 (1999) 453.
[15] B.M. Bhanage, M. Arai, Catal. Rev.: Sci. Eng. 43 (2001) 315.
[16] J.R. Hyde, P. Licence, D. Carter, M. Poliakoff, Appl. Catal. A 222 (2001) 119.
[17] W. Leitner, Acc. Chem. Res. 35 (2002) 746.
[18] E.J. Beckman, J. Supercrit. Fluid 28 (2004) 121.
[19] B. Subramaniam, M.A. McHugh, Ind. Eng. Chem. Process. Des. Dev. 25 (1986) 1.
[20] F. Zhao, S. Fujita, S. Akihara, M. Arai, J. Phys. Chem. A 109 (2005) 4419.
[21] S. Fujita, S. Akihara, F. Zhao, R. Liu, M. Hasegawa, M. Arai, J. Catal. 236 (2005) 101.
[22] S. Ichikawa, M. Tada, Y. Iwasawa, T. Ikariya, Chem. Commun. (2005) 924.
[23] J.D. Grunwaldt, R. Wandeler, A. Baiker, Catal. Rev.: Sci. Eng. 45 (2003) 1.
[24] C.M. Rayner, Org. Process Res. Dev. 11 (2007) 121.
[25] T. Seki, J.D. Grunwaldt, A. Baiker, Ind. Eng. Chem. Res. 47 (2008) 4561.
[26] F. Zhao, R. Zhang, M. Chatterjee, Y. Ikushima, M. Arai, Adv. Synth. Catal. 346 (2004) 661.
[27] F. Zhao, Y. Ikushima, M. Arai, J. Catal. 224 (2004) 479.
[28] Y. Akiyama, S. Fujita, H. Senboku, C.M. Rayner, S.A. Brough, M. Arai, J. Supercrit. Fluid 46 (2008) 197.
[29] O. Kamm, C.S. Marvel, Org. Synth. 4 (1925) 57.
[30] O. Corminboeuf, P. Renaud, Org. Lett. 4 (2002) 1731.
[31] B. Scheffer, P. Molhoek, J.A. Moulijn, Appl. Catal. 46 (1989) 11.
[32] J. Chen, Y. Li, Z. Li, X. Zhang, Appl. Catal. A 269 (2004) 179.
[33] G. Bergeret, P. Gallezot, in: G. Ertl, H. Knözinger, F. Schüth, J. Weitkamp (Eds.), Handbook of Heterogeneous Catalysis, Wiley–VCH Verlag GmbH & Co. KGaA, Weinheim, Germany, 2008, p. 738.
[34] M. Studer, S. Neto, H.U. Blaser, Top. Catal. 13 (2000) 205.
[35] G.M. Bradley, H.L. Strauss, J. Phys. Chem. 79 (1975) 1953.
[36] S. Meijers, V. Ponec, J. Catal. 160 (1996) 1.
[37] G. Vasapollo, A. Sacco, J. Organomet. Chem. 353 (1988) 119.
[38] R. Adams, E.J. Agnello, R.S. Colgrove, J. Am. Chem. Soc. 77 (1955) 5617.
[39] Y. Wu, J. Jiang, Y. Ozaki, J. Phys. Chem. A 106 (2002) 2422.
[40] Y.K. Agrawal, J. Chem. Eng. Data 22 (1977) 70.
[41] T. Seki, J.D. Grunwaldt, A. Baiker, J. Phys. Chem. B 113 (2009) 114.
[42] S.G. Kazarian, M.F. Vincent, F.V. Bright, C.L. Liotta, C.A. Eckert, J. Am. Chem. Soc. 118 (1996) 1729.
[43] J.C. Dobrowolski, M.H. Jamróz, J. Mol. Struct. 275 (1992) 211.
[44] P. Raveendran, S.L. Wallen, J. Phys. Chem. B 107 (2003) 1473.
[45] T.W. Zerda, X. Song, J. Jonas, Appl. Spectrosc. 40 (1986) 1194.

[46] J. McMurry, Organic Chemistry, Thomson Learning Inc., Belmont, 2007. p. 560.
[47] P. Politzer, J.S. Murray, M.C. Concha, Int. J. Quant. Chem. 88 (2002) 19.
[48] M.R. Nelson, R.F. Borkman, J. Phys. Chem. A 102 (1998) 7860.
[49] P. Raveendran, S.L. Wallen, J. Am. Chem. Soc. 124 (2002) 12590.
[50] X. Zhao, R. Watkins, S.W. Barton, J. Appl. Polym. Sci. 55 (1995) 773.
[51] P. Politzer, R. Bar-Adon, J. Phys. Chem. 91 (1987) 2069.
[52] P. Politzer, J.S. Murray, M.C. Concha, J. Phys. Org. Chem. 21 (2008) 155.
[53] M. Saharay, S. Balasubramanian, J. Phys. Chem. B 110 (2006) 3782.
[54] A. Vimont, A. Travert, P. Bazin, J.C. Lavalley, M. Daturi, C. Serre, G. Férey, S. Bourrelly, P.L. Llewellyn, Chem. Commun. (2007) 3291.
[55] L.M. Gonzalez, J.L. Bueno, I. Medina, Ind. Eng. Chem. Res. 40 (2001) 3711.
[56] D. Ferri, T. Bürgi, A. Baiker, Phys. Chem. Chem. Phys. 4 (2002) 2667.
[57] M. Burgener, D. Ferri, J.D. Grunwaldt, T. Mallat, A. Baiker, J. Phys. Chem. B 109 (2005) 16794.
[58] X. Ding, L.D. Rogatis, E. Vesselli, A. Baraldi, G. Comelli, R. Rosei, L. Savio, L. Vattuone, M. Rocca, P. Fornasiero, F. Ancilotto, A. Baldereschi, M. Peressi, Phys. Rev. B 76 (2007) 195425.